Hydrogen-rich Syngas Production *via* Catalytic Gasification of Sewage Sludge and Wheat Straw Using Corn Stalk Char-supported Catalysts

Shuang Shang, Chaoqiang Guo, Kui Lan, Zeshan Li, Weitao He, Zhenhua Qin, and Jianfen Li *

The co-gasification of wheat straw and wet sewage sludge for hydrogen-rich gas production was investigated in a fixed bed reactor with corn stalk char (CSC)-supported catalysts. The Ni/CSC, Ni-Fe/CSC, and Ni-Fe-La/CSC catalysts were characterized *via* ultimate analysis, X-ray fluorescence, thermogravimetric, X-ray diffraction, X-ray photoelectron spectroscopy, scanning electron microscopy, Brunauer-Emmett-Teller, and Fourier transform infrared spectroscopy analyses. A series of experiments were performed to explore the effects of reactor temperature, catalyst type, moisture content of wet sludge, and catalyst recycling performance on the composition and yield of gasification gases. The experiments demonstrated that the nickel-iron alloy ($Fe_{0.64}Ni_{0.36}$) was detected in the Ni-Fe-La/CSC catalyst, and the Ni-Fe-La/CSC catalyst showed much higher hydrogen production compared with the Ni/CSC and Ni-Fe/CSC catalysts. Furthermore, La_2O_3 effectively maintained the catalytic performance of the catalyst by relieving carbon deposition. Compared with non-catalyst biomass gasification, H_2 yield increased from 3.80 mol/kg to 11.96 mol/kg using Ni-Fe-La/CSC catalyst at 600 °C. The newly developed tri-metallic Ni-Fe-La/CSC catalyst exhibited high catalytic activity for biomass gasification at low temperature.

INTRODUCTION

At present, energy, environment, and economy are three issues that all need to be simultaneously considered. Hydrogen is a type of pollution-free energy that can reduce the reliance on oil, and it is expected to play an important role in the future energy structure. However, most of current hydrogen production is based on fossil fuel reforming (Arregi *et al.* 2018), which will release a large amount of carbon dioxide and other greenhouse gases. Therefore, it is necessary to find clean energy and renewable energy to replace fossil fuels.

Biomass is a renewable material that can be converted into solid, liquid, and gas fuels through chemical processes. The use of biomass as a fuel is a carbon neutral process. The released amount of carbon dioxide is equal to the absorbed amount of carbon dioxide *via* photosynthesis during the growth process, so the net emission of carbon dioxide is approximately zero. A large number of studies have indicated that hydrogen production *via* biomass gasification is an attractive and promising technology. Of all the thermochemical processes, steam gasification is considered to be one of the most effective techniques of generating hydrogen from biomass (Sikarwar *et al.* 2016). However, a large portion of biomass that is available for use has a high moisture content. Recently, supercritical water

bioresources.com

gasification (SCWG) has been proposed as an alternative to steam gasification for high moisture content biomass in favor of avoiding high drying costs (Arregi *et al.* 2018). Zeng *et al.* (2017) compared the difference between wet biomass self-moisture gasification (BSMG) and conventional biomass steam gasification (BSG). The results show that the water diffusion of the BSMG is spontaneous in high temperature, which leads to an increase in gas production. However, the water diffusion of BSG consumes some energy, which reduces gas production. Many researchers have studied the co-gasification of dry biomass and wet biomass used with high moisture content (Zhu *et al.* 2018). Akkache *et al.* (2016) conducted a feasibility study on the co-gasification of wastewater sludge and different feedstock. This work has shown that the concerns related to sludge gasification (pollutant release and ash fusibility) can be overcome by using the appropriate technology.

In the process of biomass gasification, a large amount of tar in the gas phase will condense at low temperature, blocking the downstream pipeline of the process, thus increasing the process cost. In addition, tar can cause a lot of energy loss and some environmental problems related to tar (Han and Kim 2008). Tar is usually highly corrosive, and its composition is complex. It is mainly composed of some toxic and harmful substances such as polycyclic aromatic hydrocarbons (PAH) and aromatic compounds (Valderrama Rios *et al.* 2018). One of the most effective techniques for removing tar is to convert it into useful gases by catalytic steam reforming, so various catalysts have been developed. Among them, metal nickel can break C–C and C–H bonds, and Ni-based catalysts are attractive in tar reforming because of their strong catalytic performance and relatively low cost. However, Ni-based catalysts are susceptible to deactivation by carbon deposition and coking during catalytic cracking. Therefore, some researchers improved the catalytic performance of Ni-based catalyst through the addition of additives such as Fe, Co, Cu, Mg, Ce, *etc.* Liu *et al.* (2010) modified the Ni/PG catalyst by adding additives (Fe, Mg, Mn, and Ce), and the results showed that Fe was the best additive for promoting the catalytic performance of Ni/PG both in tar conversion and H_2 yield. When the Fe loading was increased to 8 wt%, tar conversion was 98.2%. The traditional catalyst supports are mainly natural ores such as dolomite, olivine, and other similar ores (He *et al.* 2009).

In recent years, biochar has received increased attention due to its high specific surface area, acidic groups, and surface oxygen-containing functional groups, which play an important role in the catalytic activity of the catalyst. Biochar could effectively adsorb the light tar compounds, such as volatile organic compounds (VOCs), and the char-supported catalysts could be gasified to recover energy of char without the need for frequent regeneration after deactivation (Shen *et al.* 2016). Al-Rahbi and Williams (2017) used tire char as a catalyst for hydrogen-rich syngas production and tar reduction. Hu *et al.* (2018) prepared Ni/char catalysts by using pine sawdust char as catalyst support. The results show that the char-supported nickel catalysts have high catalytic activity in biomass gasification and tar removal. Moreover, biochar also contains alkali metals and alkaline earth metals that have a certain catalytic effect. Hu *et al.* (2015) indicated that alkaline and alkaline earth metals (AAEMs) could enhance the production of H_2 and CO_2 during biomass pyrolysis by promoting the main hydrogen production reactions such as the Boudouard reaction, the water gas shift reaction, *etc.* Yao *et al.* (2016) used wheat straw char (WC), rice husk char (RC), and cotton stalk char (CC) as catalyst supports to prepare Ni/CC, Ni/RC, and Ni/WC catalysts. The experimental results indicated that the Ni/CC catalyst showed much higher hydrogen production compared with Ni/RC and Ni/WC catalysts, due to the higher content of alkali and alkaline earth metals and the much higher external surface area.

This work aims to enhance hydrogen-rich syngas production from biomass gasification by preparing high-efficiency catalysts to support the corn stalk char. The Ni/CSC, Ni-Fe/CSC, and Ni-Fe-La/CSC catalysts were synthesized using the homogeneous precipitation method and applied to the co-gasification of wet sludge and straw. The catalysts were characterized by ultimate analysis, X-ray fluorescence (XRF), thermogravimetric (TG), X-ray diffraction (XRD), X-ray photoelectron spectroscopy (XPS), scanning electron microscopy (SEM), the Brunauer-Emmett-Teller (BET) method, and Fourier transform infrared (FTIR) spectroscopy to explore the mechanism of the catalyst. A series of experiments were performed to explore the effects of reactor temperature, catalyst type, moisture content of wet sludge, and catalyst recycling performance on the composition and yield of gasification gases. Meanwhile, a non-catalyst was also studied as the baseline for comparison.

EXPERIMENTAL

Materials

The wet sewage sludge used in this study was collected from a domestic sewage treatment plant in Wuhan, Hubei Province, China. The sludge was dried at 105 °C for 24 h in the oven to ensure that their mass was constant. Dry sludge was blended uniformly with a certain amount of water to obtain the wet sludge with different moisture contents. The wheat straw and corn stalk selected around Wuhan, China were pulverized to the size of 0.3 mm to 4.0 mm with a small crusher to eliminate the influence of the particle size on the experimental results. Corn stalk was used to prepare the chars. The biomass sample obtained by mixing wheat straw and wet sludge was used as the raw material for hydrogen-rich syngas production. The proximate and ultimate analyses of dry sludge, wheat straw, and corn stalk are listed in Table 1 and presented on an air-dried basis.

Table 1. Proximate and Ultimate Analysis of Sewage Sludge, Wheat Straw, and Corn Stalk

Sample	Proximate Analysis (wt%)				Ultimate Analysis (wt%)				
	M^{ad}	A^{ad}	V^{ad}	FC^{ad}	C	H	N	S	O^c
Sewage Sludge	4.15	50.69	35.33	9.83	25.20	5.62	3.82	0.15	14.52
Wheat Straw	10.88	6.91	67.11	15.10	31.04	4.22	0.40	0.06	57.37
Corn Stalk	11.37	8.12	68.13	12.38	32.43	4.41	0.05	0.87	54.11

M (Moisture); A (Ash); V (Volatile); FC (Fixed carbon); [ad] Air-dried; [c] Calculated by difference (O% = 100%−Ash%−C%−H%−N%−S%)

Methods

Catalysts preparation

The corn stalk char (CSC) was prepared by pyrolyzing corn stalk under nitrogen atmosphere. The reactor temperature was raised from ambient temperature to 500 °C at 10 °C/min, and then held at 500 °C for 1 h. The corn stalk char was soaked in potassium hydroxide solution for 24 h to eliminate tar. The mass ratio of char to potassium hydroxide was 3:1. Then, the corn stalk char was washed with deionized water several times followed by oven drying (105 °C).

The Ni/CSC, Ni-Fe/CSC, and Ni-Fe-La/CSC catalysts were prepared by the homogeneous precipitation method using $Ni(NO_3)_2 \cdot 6H_2O$, $Fe(NO_3)_3 \cdot 9H_2O$, and

La(NO$_3$)$_3$·6H$_2$O as nickel, iron, and lanthanum precursors, respectively. Proportions of 30 wt% of Ni, 15 wt% of Ni and Fe, and 10 wt% of Ni, Fe, and La were loaded on corn stalk char to prepare 30% Ni/CSC, 15% Ni-15% Fe/CSC, and 10% Ni-10% Fe-10% La/CSC catalysts, respectively. A certain proportion of Ni(NO$_3$)$_2$·6H$_2$O, Fe(NO$_3$)$_3$·9H$_2$O, La(NO$_3$)$_3$·6H$_2$O, and treated corn stalk char were added in a 500-mL flask. Then, 4 g potassium hydroxide as precipitant and 400 mL distilled water were added. The blend was stirred at 115 °C for 4 h. After filtering and drying overnight at 105 °C, the char-supported catalysts were devolatilized in a flowing nitrogen atmosphere from ambient temperature to 900 °C at 10 °C/min, and then they were held at 900 °C for 2 h before storage and further use.

Apparatus and procedure for biomass gasification

The experiments were performed using a fixed bed reactor facility, as shown in Fig. 1. The biomass samples and quartz wool (Daiermeng Science and Technology, Wuxi, China) containing 2 g of catalyst were placed in a porcelain boat. Before the experiment, high-purity nitrogen gas was introduced into the quartz tube for 30 min to exhaust the air in the quartz tube. The holding time was set to 10 min. Once the desired temperature was reached, the heating furnace was pushed to the position where the sample was located, and it was instantly gasified at the specified temperature. The non-condensable gases were collected with a gas collecting bag and the volume of produced gas was measured by a gas flow meter. The composition and content of the gas were measured by a gas analyzer.

Using 2.5 g of wet sludge with a moisture content of 60 wt% and 1 g of wheat straw as biomass material, different kinds of catalysts were added and gasified at 600 °C, 700 °C, 800 °C, and 900 °C, to explore the influence of temperature and catalyst type. A sample of 1 g of wheat straw was separately mixed with wet sludge (the dry sludge was 1 g) with moisture contents of 30 wt%, 40 wt%, 50 wt%, 60 wt%, 70 wt%, and 80 wt%, and gasified at 600 °C using the Ni-Fe-La/CSC catalyst, to consider the influence of moisture content. A sample of 2.5 g of wet sludge with a moisture content of 60 wt% and 1 g of wheat straw were used as biomass material and gasified at 600 °C. The biomass material was changed after each experiment, and the catalysts were used repeatedly to consider the influence of the catalyst recycling performance.
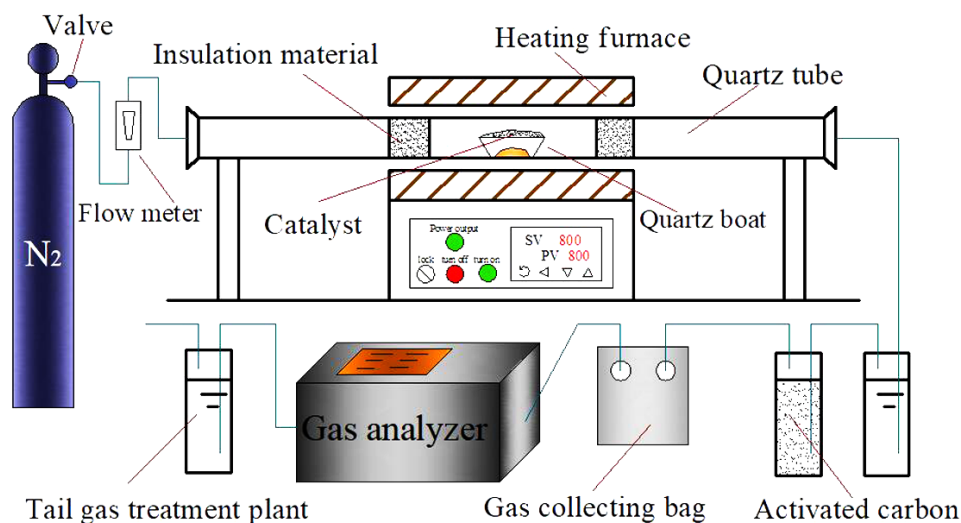
Fig. 1. Schematic diagram of the experimental system

bioresources.com

Analysis

The ultimate analysis of the samples was conducted using a CHNS/O analyzer (FLASH2000, Thermo Fisher Scientific, Waltham, MA, USA). This analysis gave the mass percentages of carbon, hydrogen, nitrogen, and sulfur in the samples simultaneously, and the mass percent of oxygen was determined by difference. The proximate analysis method of coal, according to GB/T 212 (2008), was used to obtain proximate analysis of the sewage sludge, wheat straw, and corn stalk (*i.e.*, moisture, volatile matter, fixed carbon, and ash content of the material). The element composition and material structure of the catalyst were analyzed using an X-ray fluorescence spectrometer (EDX-7000; Shimadzu Corp., Kyoto, Japan) and an X-ray diffractometer (XRD-7000; Shimadzu Corp., Kyoto, Japan). The thermal stability of the support and catalyst were evaluated using a thermogravimetric analyzer (SDT Q600; TA Instruments, New Castle, DE, USA). The XPS analysis (DLD-600W; Shimadzu Corp., Kyoto, Japan) was used to qualitatively analyze the surface elements of the catalyst and their valence states. Scanning electron microscopy (S-3000N; Hitachi, Ltd., Tokyo, Japan) was used to observe the surface morphology of the support and catalyst. Surface area and pore properties of the support and catalyst were determined by a surface area analyzer (ASAP 2020 HD88; Micromeritics Instrument Corp., Norcross, GA, USA). The chemical functional groups in catalyst samples were investigated using FTIR (Nicolet IS10; Thermo Fisher Scientific, Waltham, MA, USA). The gas composition analysis was conducted with an infrared gas analyzer (Gasboard-3100P; Hubei Cubic-Ruiyi Instrument Co., Wuhan, China).

The lower heating value (LHV) of the product gas is defined by Lv *et al.* (2004) as follows,

$$LHV \, (kJ/Nm^3) = (27.5 \times H_2 + 30 \times CO + 85.4 \times CH_4 + 151.3 \times C_nH_m) \times 4.2$$
$$(1)$$

where H_2, CO, CH_4, and C_nH_m are the gas component concentrations of the product gas.

RESULTS AND DISCUSSION

Characterization of Catalysts
Ultimate analysis and XRF

Table 2 shows the components of CSC, Ni/CSC, used Ni/CSC, Ni-Fe/CSC, used Ni-Fe/CSC, Ni-Fe-La/CSC, and used Ni-Fe-La/CSC. It shows that the corn stalk char was mainly composed of C, K, Si, Ca, and Fe. Because the biochar was soaked in a potassium hydroxide solution for 24 h to remove tar, the K content in the CSC was high. During preparation of the catalysts, potassium decomposed at high temperature, which resulted in low potassium content in the catalysts. According to the results of XRF analysis, nickel, iron, and lanthanum had been successfully loaded on the char support. It could be seen from the ultimate analysis results that the carbon content in the catalyst was lower than that in the char support. Firstly, the char support was prepared for 500 °C, while the catalyst was calcined at 900 °C. Secondly, due to the catalysis of metals, CO_2 was formed by C and O during the preparation of catalyst, which resulted in the decrease of C content in the catalyst. Additionally, the C content in the catalysts increased slightly after reaction. On the one hand, it was caused by carbon deposition on the surface of the catalyst. On the other hand, the oxygen element of metal oxide was removed by the reduction reaction. The mass loss of oxygen element will also increase the carbon content in the catalyst after reaction.

bioresources.com

After the three catalysts were used an equal amount of times, the carbon deposition of Ni-Fe-La/CSC catalyst was the least.

Table 2. Ultimate Analysis and XRF Analysis of Seven Samples

Sample	Main Composition and Content (%)							
	C	H	Ni	Fe	La	Si	K	Ca
CSC	60.81	0.96	—	2.99	—	10.11	11.65	9.70
Ni/CSC	42.13	0.36	44.52	0.34	—	5.51	3.77	2.23
Used Ni/CSC	43.66	0.22	43.28	0.31	—	6.07	2.73	2.03
Ni-Fe/CSC	43.86	0.39	23.21	21.47	—	4.01	0.86	0.68
Used Ni-Fe/CSC	44.92	0.34	22.35	20.88	—	5.22	0.76	0.63
Ni-Fe-La/CSC	43.14	0.42	13.52	13.73	15.18	4.45	4.93	1.72
Used Ni-Fe-La/CSC	43.96	0.35	13.01	13.10	14.36	4.58	3.81	1.49

TG analysis

Figure 2 shows the thermogravimetric analysis of char support and char-supported catalysts under the N_2 atmosphere. With the test temperature rising from ambient temperature to 900 °C, the mass loss of Ni/CSC catalyst and Ni-Fe-La/CSC catalyst was only about 15 wt%, in which the water loss was 5 wt%. However, the mass loss of the Ni-Fe/CSC catalyst reached 23%. Consequently, the Ni/CSC catalyst and Ni-Fe-La/CSC catalyst had high thermal stability, while the thermal stability of the Ni-Fe/CSC catalyst was poor. In addition, the mass of char support decreased remarkably with the increase of test temperature, and the maximum mass loss reached 40 wt% when the temperature was 900 °C. Because the char support was prepared for 500 °C, the mass loss was lower before 500 °C, and the mass of CSC was remarkably reduced after 500 °C.
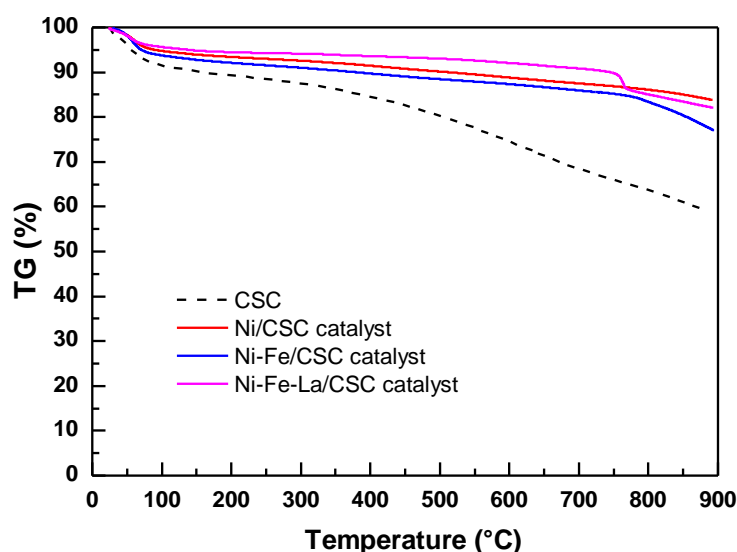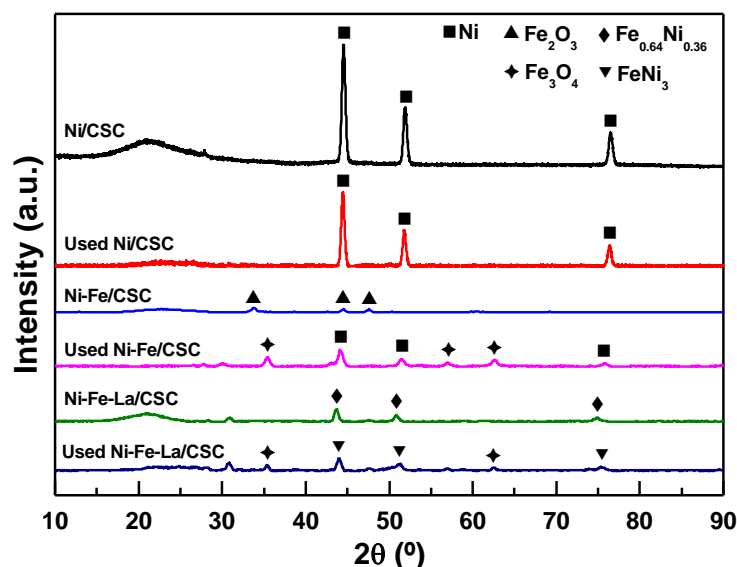

Fig. 2. TG analysis of char support and char-supported catalysts under the N_2 atmosphere

XRD analysis

Figure 3 shows the XRD patterns of char-supported catalysts and used catalysts. The characteristic diffraction peaks of Ni (111), Ni (200), and Ni (220) at $2\theta = 44.2°$, $51.8°$, and $76.1°$, respectively, were observed in the Ni/CSC catalyst, which showed a better crystalline structure. Some weak characteristic diffraction peaks of Fe_2O_3 were observed

in the Ni-Fe/CSC catalyst. According to XRF analysis, a certain amount of nickel and iron had been loaded into the Ni-Fe/CSC catalyst. However, the characteristic peaks of Ni^0 and NiO were not found over the Ni-Fe/CSC catalyst, which was attributed to the high dispersion or poor crystallinity of nickel. The strong peak at $2\theta = 41.8°$, $50.3°$, and $72.2°$ was observed and identified as an alloy of Ni-Fe ($Fe_{0.64}Ni_{0.36}$). No La_2O_3 diffraction peak was detected in the Ni-Fe-La/CSC catalyst, which indicated a high dispersion of La_2O_3 in the catalyst.

Except for the Ni/CSC catalyst, the active components of the Ni-Fe/CSC and Ni-Fe-La/CSC catalysts had undergone corresponding changes after 10 instances of reuse, and thus affected the catalytic activity of the catalyst. The reasoning might be that the reducing gas, such as H_2 and CO, generated during the catalytic gasification of the biomass maintained the active component of the Ni/CSC catalyst as Ni^0. The active components of the Ni-Fe/CSC catalyst were reduced from Fe_2O_3 and NiO to Fe_3O_4 and Ni^0, respectively. Moreover, although the active component of the Ni-Fe-La/CSC catalyst was converted from $Fe_{0.64}Ni_{0.36}$ to $FeNi_3$ and Fe_3O_4, the active component was still mainly nickel-iron alloy.
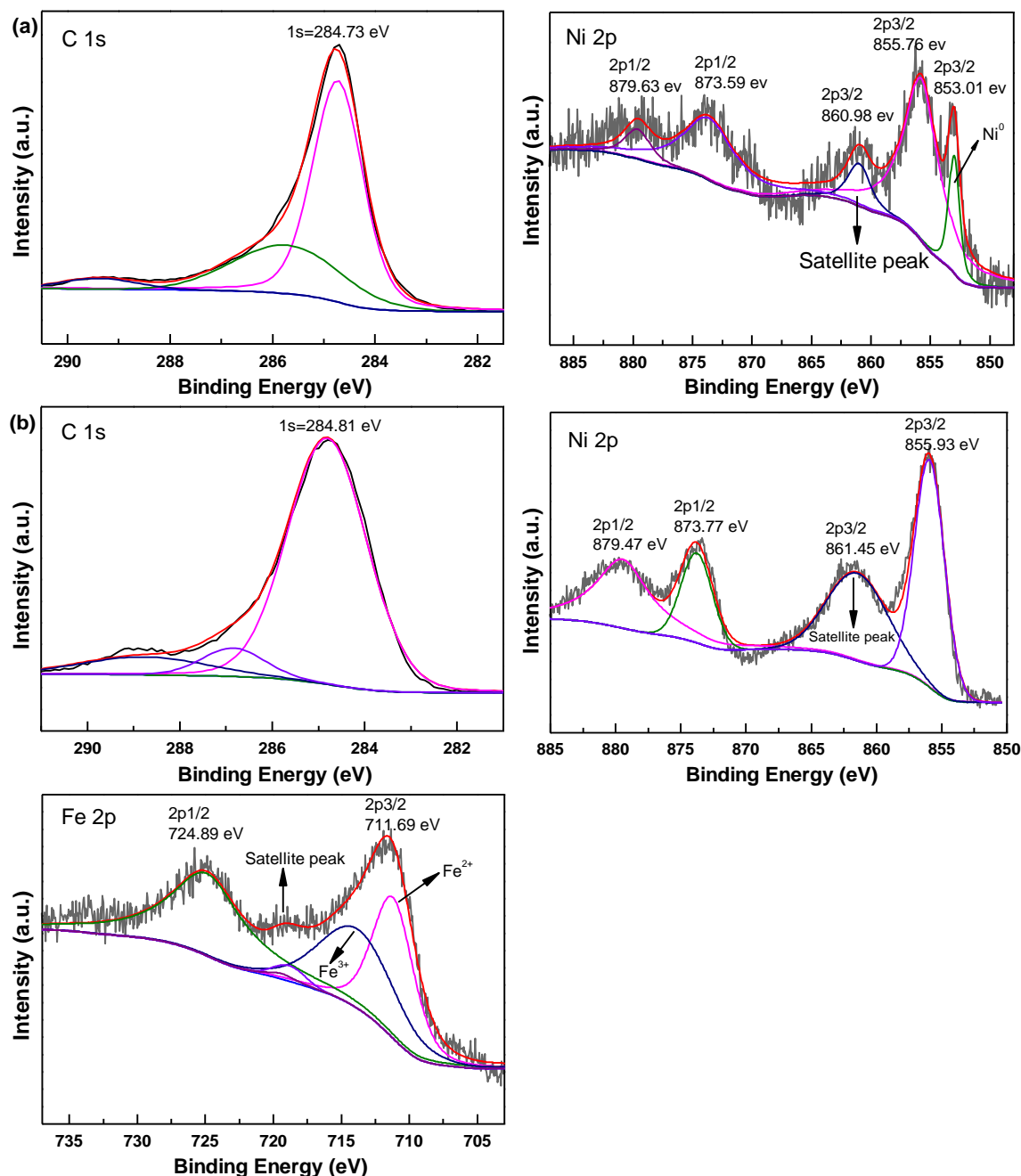

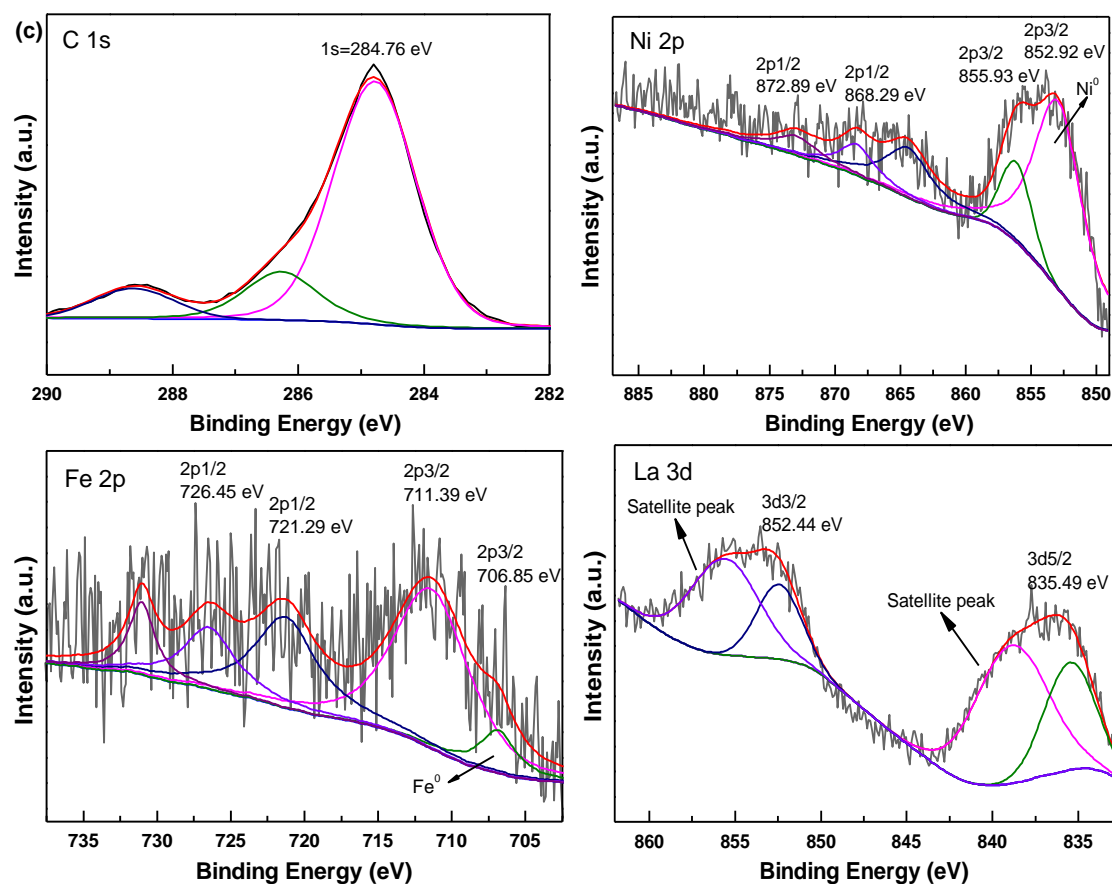**Fig. 3.** XRD patterns of char-supported catalysts and used catalysts

XPS analysis

Figure 4 shows the XPS patterns of Ni/CSC, Ni-Fe/CSC, and Ni-Fe-La/CSC catalysts. The XPS patterns of C1s and Ni 2p regions for the Ni/CSC catalyst are depicted in Fig. 4(a), with the curve-fitting spectra included. Figure 4(a) shows the binding energy of C1s distributed at 284.73 eV in the spectrum. In general, charging effects were corrected by adjusting the binding energy of C1s to 284.6 eV. Therefore, the binding energy of all elements should be calibrated by subtracting 0.13 eV. The Ni 2p3/2 peak of Ni/CSC catalyst at 853.01 eV was the characteristic peak of Ni^0, which was in agreement with the results of the XRD analysis. In addition, the Ni 2p3/2 peak of Ni/CSC catalyst at 855.76 eV was attributed to the strong interaction with compounds, such as SiO_2 and Fe_2O_3, formed $NiSiO_3$ and $NiFe_2O_4$.

As shown in Fig. 4(b), the peak of Ni^0 disappeared in the spectrum of the Ni-Fe/CSC catalyst, which indicated that there was no Ni^0 present in the Ni-Fe/CSC catalyst.

bioresources.com

This conclusion was also confirmed by the fact that no peak of nickel was observed in the XRD pattern. The binding energy of Ni 2p3/2 at 855.93 eV was identified as the peak of $NiFe_2O_4$, $Ni(OH)_2$, and Ni_2O_3. Furthermore, the binding energy of Fe 2p3/2 at 711.69 eV was identified as the peak of Fe_2O_3 and FeO(OH). The Fe 2p3/2 peak had associated satellite peaks.

Fig. 4. XPS patterns of char-supported catalysts: (a) Ni/CSC catalyst, (b) Ni-Fe/CSC catalyst, and (c) Ni-Fe-La/CSC catalyst

The satellite peak of Fe 2p3/2 for Fe_2O_3 was located approximately 8 eV higher than the main Fe 2p3/2 peak (Yamashita and Hayes 2008), which was clearly shown in the spectrum. In the XRD spectrum, the weak peak of Fe_2O_3 was also observed. The binding energies at 709.89 eV and 714.33 eV were identified as the peaks of Fe^{2+} and Fe^{3+} (He *et al.* 2018). Additionally, the Fe 2p3/2 signal showed that the binding energy of the divalent oxide state of Fe at 709.89 eV was the main signal recorded. The peak at 714.33 eV corresponded to the trivalent-oxide state of Fe. The other peaks correspond to satellites of Fe^{2+} and Fe^{3+}. Therefore, FeO was contained in the Ni-Fe/CSC catalyst.

As shown in Fig. 4(c), the binding energies of Ni 2p3/2 at 852.92 eV and Fe 2p3/2 at 706.85 eV were identified as the peaks of Ni^0 and Fe^0, respectively. According to the XRD pattern of the Ni-Fe-La/CSC catalyst, the alloy of Ni-Fe ($Fe_{0.64}Ni_{0.36}$) was formed in the catalyst. Consequently, the characteristic peaks of Ni^0 and Fe^0 were observed in the XPS patterns, which also indicated the presence of Ni-Fe alloy. The XPS pattern of the La 3d region showed that the deconvolution of the La 3d spectrum with four lines corresponded to spin-orbit splitting (La 3d3/2 and La 3d5/2) and their shake-up satellites at higher binding energy sites (Sienkiewicz-Gromiuk *et al.* 2016). The binding energy of La 3d5/2 at 835.49 eV was identified as the peak of La_2O_3. Mazumder and De Lasa (2014) showed that La_2O_3 could increase the reducible nickel by reducing the formation of $NiAl_2O_4$ spinel, and increase the dispersibility of nickel by reducing the interaction between the metal and the support. In the Ni-Fe-La/CSC catalyst, the presence of La_2O_3

could increase the dispersibility of the metal and the active site of the catalyst, thus affecting the catalytic performance of the catalyst.

SEM analysis

Taking the Ni-Fe-La/CSC catalyst as an example, Fig. 5 shows the SEM images of CSC, Ni-Fe-La/CSC catalyst, and used Ni-Fe-La/CSC catalyst. Figure 5(a) shows that the corn stalk became a highly porous carbonaceous material after high temperature pyrolysis. The char support had high adsorption performance due to its uniform structure and developed pores, which resulted in the good residence time of tar reacting with the catalyst. The char support could effectively adsorb tar and crack it on the metal surface, which then increased the content of H_2 in the product gas. Figure 5(b) shows that there were some small particles on the surface of the support. Therefore, it can be speculated that the metal had been successfully supported on the surface, and the pore structure was still clean and visible. However, Fig. 5(c) shows that the particles on the surface of the support became larger than before use, which indicated that the use of the catalyst at high temperature for a long time made the metal agglomerate. According to Scherrer formula, the average size of nickel iron alloy grains in the Ni-Fe-La/CSC catalyst increased from 15 nm to 17 nm after 10 instances of reuse. Additionally, the pore structure of the support was also unclear, which was attributed to the carbon deposition of the catalyst blocking the void.

Fig. 5. SEM images of (a) CSC, (b) Ni-Fe-La/CSC catalyst, and (c) used Ni-Fe-La/CSC catalyst

BET analysis

The textural parameters of CSC, catalysts, and used catalysts, including BET surface area, total pore volume, and average pore diameter, are listed in Table 3. The data show that BET surface area of Ni-Fe/CSC (197.25 m^2/g) was the highest among these three catalysts, and that BET surface area of Ni/CSC was the smallest (16.49 m^2/g). It might have been attributed to the worst thermal stability of Ni-Fe/CSC catalyst, which resulted in a larger specific surface area during catalyst preparation.

Table 3. Textural Parameters of CSC, Catalysts, and Used Catalysts

Sample	BET Surface Area (m^2/g)	Total Pore Volume (cm^3/g)	Average Pore Diameter (nm)
CSC	16.27	0.030	53.36
Ni/CSC	16.49	0.035	49.14
Used Ni/CSC	2.62	0.011	127.21
Ni-Fe/CSC	197.25	0.246	26.15
Used Ni-Fe/CSC	9.79	0.037	69.74
Ni-Fe-La/CSC	73.69	0.130	43.57
Used Ni-Fe-La/CSC	5.70	0.050	150.78

Furthermore, it was found that the BET surface area and pore volume of the catalyst decreased after 10 instances of reuse. Carbon deposition of the catalyst would block some micropores, which would result in a decrease in the BET surface area. Compared with the fresh catalysts, the used catalysts had a larger pore diameter due to the constant consumption of the char-supported catalyst during reuse. In addition, all three catalysts had a mesoporous structure, which also indicated that they had strong performances for adsorption.

FTIR analysis

Figure 6 shows the FTIR spectra of CSC, Ni/CSC, Ni-Fe/CSC, and Ni-Fe-La/CSC catalysts. A large number of studies have shown that biochar can adsorb tar produced during biomass gasification (Paethanom *et al.* 2012, 2013). The mechanism of tar adsorption by biochar is complex, which is related not only to the pore structure of biochar, but also to the functional groups on the surface of biochar. There was a strong and wide absorption band between 3250 cm^{-1} and 3750 cm^{-1}, which was identified as –OH stretching vibrations. The peak at 3200 cm^{-1} was likely indicative of –NH_2 stretching vibrations. Additionally, –NH_2 was a basic functional group, while phenol was a Lewis acid. Therefore, phenol can easily combine with –NH_2 *via* the acid-base interaction (Shen *et al.* 2016), and thereby be adsorbed by biochar. Then, it will undergo catalytic cracking reaction at the active site on the char-supported catalyst. The peaks at 1100 cm^{-1} and 1700 cm^{-1} were likely indicative of C–O and C=O stretching vibrations, respectively. Some organic functional groups, such as –OH, C–O, and C=O, can interact with phenol *via* hydrogen bonds. Moreover, the chemical interaction between the functional group and the phenol molecule can effectively enhance the adsorption (Liu *et al.* 2011).
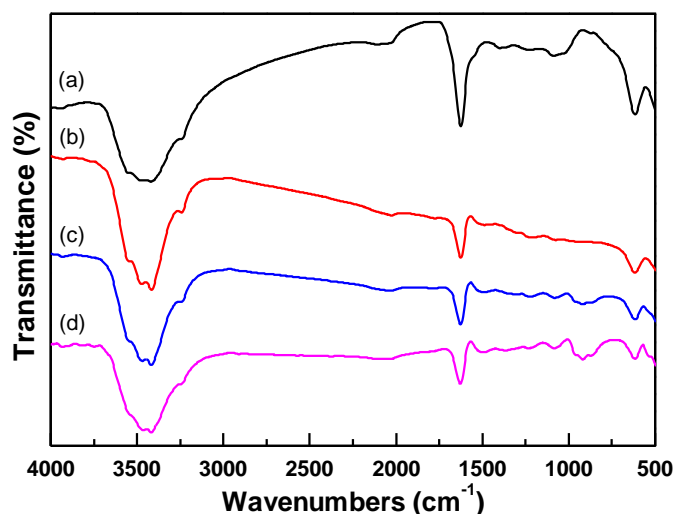
Fig. 6. FTIR spectra of CSC and char-support catalysts: (a) CSC, (b) Ni/CSC, (c) Ni-Fe/CSC, and (d) Ni-Fe-La/CSC

Catalytic Performance of Ni/CSC, Ni-Fe/CSC, and Ni-Fe-La/CSC Catalysts

Reactor temperature, catalyst type, moisture content of wet sludge, and catalyst recycling performance were explored in this experiment. The catalytic activity of catalysts in biomass gasification was evaluated through comparing H_2 and CO content in the product gas. The important reactions taking place during catalytic gasification of wet sludge and straw are summarized as follows (Yang *et al.* 2018):

Drying process: Wet sample → steam + dry sample (2)

Pyrolysis: Dry sample → gas + tar + char (3)

Secondary cracking: $Tar → H_2 + CO + CO_2 + CH_4 + H_2O + C_nH_m$ (4)

Steam gasification reaction: $C_nH_m + nH_2O + Q → nCO + [n + (m/2)]H_2$ (5)

Methane reforming reaction: $CH_4 + H_2O → CO + 3H_2 + 206$ kJ/mol (6)

Water gas shift reaction: $CO + H_2O → CO_2 + H_2 - 41$ kJ/mol (7)

Char steam gasification reaction: $C + H_2O → CO + H_2 + 131$ kJ/mol (8)

Boudouard reaction: $C + CO_2 → 2CO + 172$ kJ/mol (9)

Figure 7 shows the processes of biomass catalytic gasification and catalyst preparation. First, what happened to the wet sample at high temperature was the drying process, which formed *in-situ* steam around the sample (Eq. 2). Meanwhile, the dry sample was rapidly pyrolyzed to gas, tar, and char (Eq. 3), followed by secondary cracking of tar to form gas and small molecule organic matter (Eq. 4), steam gasification reaction, methane reforming reaction, water gas shift reaction, char steam gasification reaction, and Boudouard reaction (Eqs. 5 through 9). The primary gas was produced from the thermal scission of chemical bonds in the individual constituents of biomass, when catalytic reforming reactions cleaved the C–C and C–H bonds of the carbohydrate backbone to produce CO and H_2 (Kunkes *et al.* 2008). Due to the presence of *in-situ* steam, char steam gasification reaction could not only refresh the active surface area of catalyst by reducing the carbon deposit of the catalyst, but also increase the CO and H_2 content in the gas.
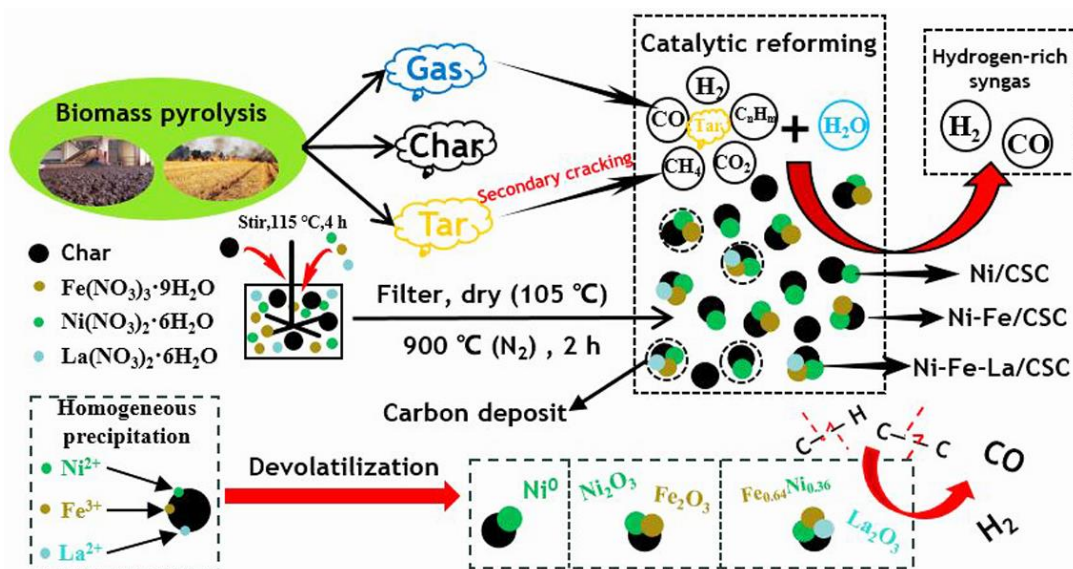
Fig. 7. Processes of catalytic gasification of biomass using Ni/CSC, Ni-Fe/CSC, and Ni-Fe-La/CSC catalysts

Influence of reactor temperature on gas composition

The reactor temperature played an important role in the co-gasification of wet sludge and straw, because the decomposition temperatures of various components, such as hemicellulose, cellulose, lignin, aliphatic compounds, and proteins, were different, and the process was an endothermic reaction. It could be seen from Fig. 8 that the trends of gas composition change were almost the same regardless of the catalyst. The contents of H_2 and CO increased gradually with the increase of reactor temperature while the contents of CH_4 and CO_2 decreased. Yang *et al.* (2018) have studied the co-gasification of wet sludge and sawdust and found the same trend, which was attributed to higher temperature providing more favorable conditions for thermal cracking of hydrocarbon. Taking Fig. 8(c) as an example, the content of H_2 increased from 32.03 vol% to 46.89 vol%, a 46.39% relative increase. At the same time, the CO content increased from 26.32 vol% to 34.34 vol%, a 30.47% relative increase. The main reason for this phenomenon was that the cracking of cycloalkanes and the breaking of the long chains of macromolecules would be gradually increased with the increase of reactor temperature. Additionally, according to Le Chatelier's principle, higher temperature was favorable for increasing products in the endothermic reactions and reactants in the exothermic reactions. In other words, raising the reactor temperature promoted the steam gasification reaction of hydrocarbon, methane reforming reaction, char steam gasification reaction, and Boudouard reaction. Moreover, the water gas shift reaction was suppressed. Thereby, a large number of hydrocarbons, CO_2, and CH_4 were consumed and converted into H_2 and CO, and CO was prevented from being converted to CO_2.
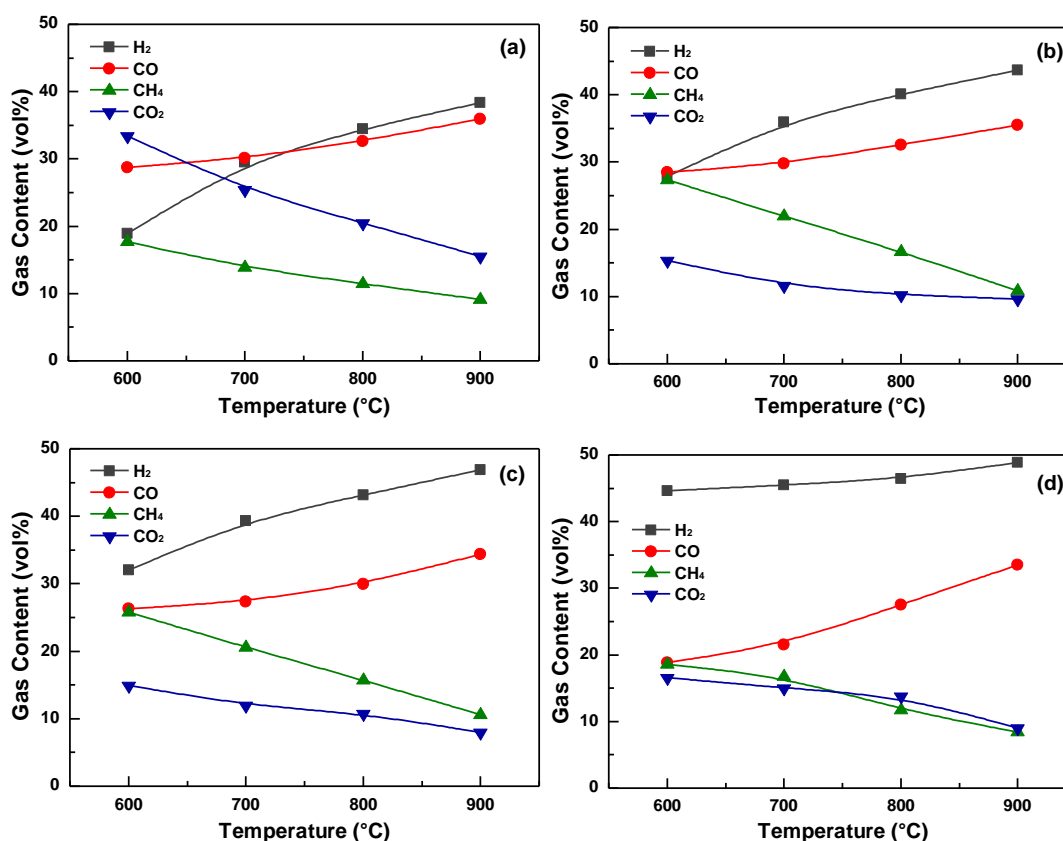
Fig. 8. Influence of reactor temperature on gas composition: (a) No catalyst, (b) Ni/CSC, (c) Ni-Fe/CSC, and (d) Ni-Fe-La/CSC

bioresources.com

Influence of the catalyst on syngas

As shown in Fig. 9, compared with the dry sample, the wet sample could form *in-situ* steam during gasification to increase the H_2 content in the gas phase. With higher reactor temperatures, the effect was more noticeable, which could be explained by the process from Eqs. 5 through 9. In addition, in the absence of the catalyst, the CO content was higher than that of H_2. However, the content of H_2 was remarkably higher than that of CO when the catalyst was used. This indicated that the catalysts played a crucial role in the process of biomass gasification that was prepared hydrogen-rich syngas.
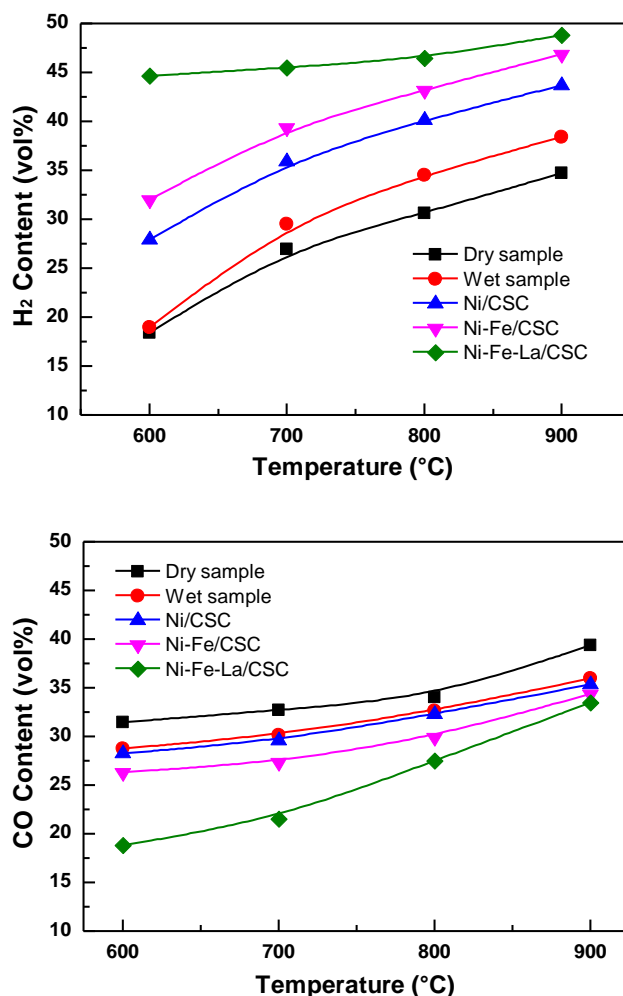

Fig. 9. Influence of the catalyst on syngas

Table 4 shows gas composition, dry gas yield, H_2 yield, and LHV from catalytic *in-situ* steam gasification of biomass with different catalysts. It shows that the dry gas yield, H_2 yield, and LHV at 600 °C *in-situ* steam gasification in the absence of catalyst were 0.45 $N·m^3/kg$, 3.80 mol/kg, and 18.56 $MJ/N•m^3$, respectively. The Ni-Fe-La/CSC catalyst showed the highest catalytic activity for dry gas yield (0.60 $N·m^3/kg$) and H_2 yield (11.96 mol/kg) compared with the Ni/CSC and Ni-Fe/CSC catalysts. However, the LHV (15.03 $MJ/N·m^3$) of gas was the lowest, which resulted from the fact that CH_4 and C_nH_m had much higher calorific values than H_2 or CO. As shown in Fig. 9, regardless of the reactor temperature, Ni-Fe-La/CSC catalyst showed the best catalytic effect due to the presence of

nickel-iron alloy ($Fe_{0.64}Ni_{0.36}$). Xie *et al.* (2018) prepared nanofiber-supported Fe-Ni bimetallic catalysts for biomass gasification. The results showed that the $Fe_{0.64}Ni_{0.36}$ alloy detected in the Fe-Ni/carbon nanofibers catalyst had a remarkably high catalytic ability to aromatic compounds. Moreover, the catalytic effect of the Ni-Fe/CSC catalyst was better than that of the Ni/CSC catalyst because the oxide of iron in the Ni-Fe/CSC catalyst contributed to the generation of H_2 and the gasification reaction (Shen *et al.* 2014). The catalytic effect of Ni-Fe-La/CSC catalyst was not noticeably improved at high temperature compared with Ni/CSC and Ni-Fe/CSC catalysts, but the catalytic effect of Ni-Fe-La/CSC catalyst was remarkably improved at low temperature. For example, compared with the case without catalyst, when the temperature was 600 °C, the H_2 content after using Ni-Fe-La/CSC catalyst increased from 18.93 vol% to 44.65 vol%, a 135.87% relative increase. However, when the temperature was 900 °C, the content of H_2 increased from 38.41 vol% to 48.84 vol%, a 27.15% relative increase. At the same time, with the increase of temperature, for the Ni-Fe-La/CSC catalyst, the tendency of H_2 content to increase was relatively flat. According to Fig. 5, it could be speculated that the metal was agglomerated at high temperature, which affected the active surface area of the catalyst. In conclusion, the newly developed Ni-Fe-La/CSC catalyst showed high application value in the production of valuable gas in biomass cryogenic gasification. When the catalytic temperature was 600 °C, the H_2 yield reached 11.96 mol/kg.

Table 4. Influence of Catalyst on Gas Composition and Gas Characterization

Catalyst	No Catalyst	Ni/CSC	Ni-Fe/CSC	Ni-Fe-La/CSC
Gasification Temperature (°C)	600	600	600	600
Catalytic Temperature (°C)	600	600	600	600
H_2 Content (vol%)	18.93	27.89	32.03	44.65
CO Content (vol%)	28.72	28.45	26.32	18.84
CH_4 Content (vol%)	33.39	27.34	25.80	18.61
CO_2 Content (vol%)	17.73	15.37	14.89	16.62
C_nH_m Content (vol%)	1.23	0.95	0.95	1.29
Dry Gas Yield ($N·m^3$/kg)	0.45	0.53	0.56	0.60
H_2 Yield (mol/kg)	3.80	6.60	8.01	11.96
LHV ($MJ/N·m^3$)	18.56	17.22	16.87	15.03

Influence of moisture content of wet sludge on syngas

The wet sludge (the dry sludge was 1 g) with moisture contents of 30 wt%, 40 wt%, 50 wt%, 60 wt%, 70 wt%, and 80 wt% were separately blended uniformly with 1 g straw, and the moisture content of the blended biomass samples were 17.7 wt%, 25.1 wt%, 33.3 wt%, 42.86 wt%, 53.81 wt%, and 66.67 wt%, respectively. Then, the samples were gasified at 600 °C using the Ni-Fe-La/CSC catalyst. Figure 10 shows the influence of moisture content of wet sludge on syngas and H_2 yield.

It was shown that the H_2 content and H_2 yield showed a trend of first increasing and then decreasing as the moisture content of wet sludge increased. As the moisture content of wet sludge increased from 30 wt% to 60 wt%, the H_2 content gradually increased from 38.81 vol% to 44.65 vol%, and the H_2 yield increased from 9.44 mol/kg to 11.96 mol/kg. When the moisture content was further increased from 60 wt% to 80 wt%, the H_2 content declined from a maximum value of 44.65 vol% to 38.27 vol%, and the H_2 yield decreased from 11.96 mol/kg to 11.10 mol/kg. The variations emerged because *in-situ* steam was used as a gasifying agent, which could promote steam gasification, methane reforming, water gas shift, and char steam gasification reactions (Eqs. 5 through 8) and thereby

increase the content of H_2. However, with the increase of moisture content of wet sludge, more heat would be needed for endothermic reaction. What's more, excess steam would consume more energy and limit heat transfer between the heating furnace and the biomass, which might make gasification temperature lower than theoretical temperature. In addition, the CO content gradually decreased with the increase of moisture content of wet sludge. The possible reason was that the increasing steam concentration promoted the water gas shift reaction (Eq. 7) to consume CO. In conclusion, when the moisture content of the mixed biomass was approximately 40 wt%, both the H_2 content (44.65 vol%) and H_2 yield (11.96 mol/kg) reached the maximum.
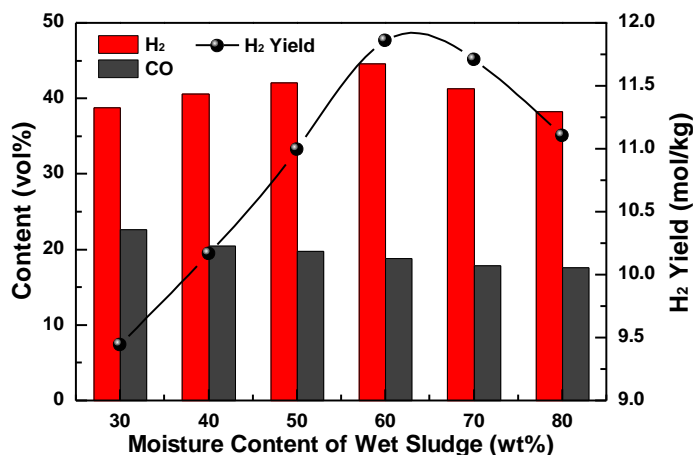

Fig. 10. Influence of moisture content of wet sludge on syngas and H_2 yield

Catalyst cyclability

The testing results of the 10-cycling that used Ni/CSC, Ni-Fe/CSC, and Ni-Fe-La/CSC catalysts are shown in Fig. 11. The figure shows that the catalytic performance of the catalyst and the H_2 content tended to decrease with the increase of cycle test times. Additionally, the catalytic effects of Ni-Fe/CSC and Ni-Fe-La/CSC catalyst tended to be stable after 8 and 4 instances of reuse, while the catalytic effect of the Ni/CSC catalyst kept declining. After 10 instances of reuse, the H_2 content decreased by 5.29%, 9.51%, and 11.77%, respectively, which indicated that the Ni-Fe-La/CSC catalysts exhibited stable catalytic performance. As shown in Table 2, the carbon deposition of the Ni-Fe-La/CSC catalyst was the lowest. Al-Fatesh *et al.* (2014) showed that La_2O_3 could decrease the acidity of the support, thereby stopped pyrolytic carbon formation, and the basic La_2O_3 favored the chemisorption and dissociation of CO_2 and reverse Boudouard reaction. Therefore, La_2O_3 could extend the usage time of Ni-Fe-La/CSC catalyst by reducing the carbon deposition. Another reason was that the active components of Ni-Fe-La/CSC catalyst had not changed and it was still nickel-iron alloy after reuse. However, the active components of Ni-Fe/CSC catalyst were converted from Fe_2O_3 and NiO to Fe_3O_4 and Ni^0, respectively, which would consume reducing gases, such as H_2 and CO, which resulted in the decrease of H_2 content in the product gas. Although the active component of Ni/CSC catalyst was always Ni^0, the content of H_2 in the gas phase gradually decreased, even lower than that without catalyst after 7 instances of reuse. It could be speculated that the active component of Ni/CSC catalyst was not always Ni^0 while it was converted between NiO and Ni^0. Once NiO was produced, it would be reduced to Ni^0 by H_2 and CO, which resulted in a gradual decrease of H_2 content in the gas phase.
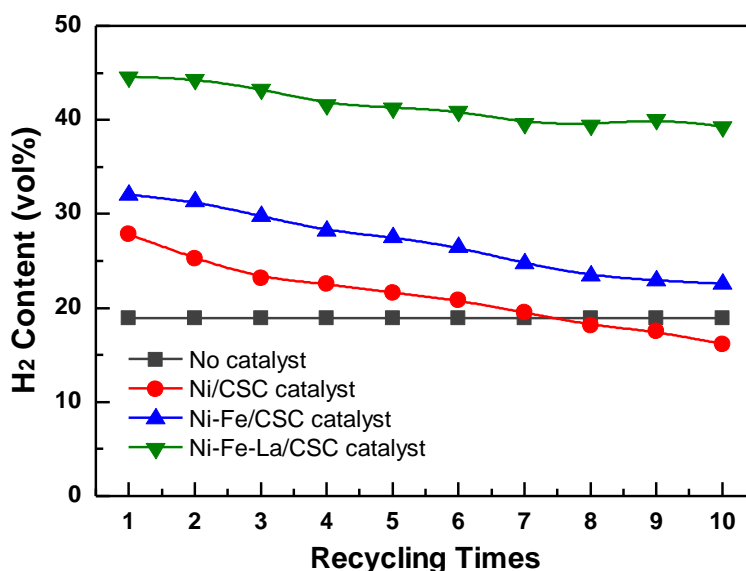
Fig. 11. The H_2 content of cycling test with Ni/CSC, Ni-Fe/CSC, and Ni-Fe-La/CSC catalysts

CONCLUSIONS

1. After 10 instances of reuse, there was a slight deposition of coke on the surface of catalysts, and the carbon deposition of Ni-Fe-La/CSC catalyst was the least, followed by Ni-Fe/CSC catalyst and Ni/CSC catalyst.

2. The Ni/CSC and Ni-Fe-La/CSC catalysts exhibited high thermal stability, but the thermal stability of the Ni-Fe/CSC catalyst and char support were poor. The maximum mass loss of char support reached 40 wt%.

3. Except for the Ni/CSC catalyst, the active components of the Ni-Fe/CSC and Ni-Fe-La/CSC catalysts had undergone corresponding changes after 10 instances of reuse, and thus affected the catalytic activity of the catalyst.

4. Both char support and char-supported catalysts had abundant mesoporous structure and surface functional groups, and the BET surface area and pore volume of the catalysts decreased after 10 instances of reuse.

5. Long time use of catalyst at high temperature will make the metal agglomerate. The average size of nickel iron alloy grains in the Ni-Fe-La/CSC catalyst increased from 15 nm to 17 nm after 10 instances of reuse.

6. Higher temperature could promote the syngas production. With the addition of the Ni/CSC, Ni-Fe/CSC and Ni-Fe-La/CSC catalyst, the H_2 yield increased from 3.80 mol/kg to 6.60 mol/kg, 8.01 mol/kg and 11.96 mol/kg, respectively.

7. The H_2 content and H_2 yield showed a trend of first increasing and then decreasing as the moisture content of wet sludge increased. When the moisture content of the mixed biomass was approximately 40 wt%, both the H_2 content and H_2 yield reached the maximum.

bioresources.com

8. The Ni-Fe-La/CSC catalyst exhibited stable catalytic performance. After 10 instances of reuse, the H_2 content only decreased by 5.29%. However, the stable cyclability of Ni/CSC and Ni-Fe/CSC catalysts were poor.

ACKNOWLEDGMENTS

REFERENCES CITED

Akkache, S., Hernández, A.-B., Teixeira, G., Gelix, F., Roche, N., and Ferrasse, J. H. (2016). "Co-gasification of usedwater sludge and different feedstock: Feasibility study," *Biomass Bioenerg.* 89, 201-209. DOI: 10.1016/j.biombioe.2016.03.003

Al-Fatesh, A. S., Naeem, M. A., Fakeeha, A. H. and Abasaeed, A. E. (2014). "Role of La_2O_3 as promoter and support in Ni/γ-Al_2O_3 catalysts for dry reforming of methane," *Chin. J. Chem. Eng.* 221, 28-37. DOI: 10.1016/S1004-9541(14)60029-X.

Al-Rahbi, A. S., and Williams, P. T. (2017). "Hydrogen-rich syngas production and tar removal from biomass gasification using sacrificial tyre pyrolysis char," *Appl. Energ.* 190, 501-509. DOI: 10.1016/j.apenergy.2016.12.099

Arregi, A., Amutio, M., Lopez, G., Bilbao, J., and Olazar, M. (2018). "Evaluation of thermochemical routes for hydrogen production from biomass: A review," *Energ. Convers. Manage.* 165, 696-719. DOI: 10.1016/j.enconman.2018.03.089

GB/T 212 (2008). "Proximate analysis of coal," Standardization Administration of China, Beijing, China.

Han, J., and Kim, H. (2008). "The reduction and control technology of tar during biomass gasification/pyrolysis: An overview," *Renew. Sust. Energ. Rev.* 12(2), 397-416. DOI: 10.1016/j.rser.2006.07.015

He, M., Hu, Z., Xiao, B., Li, J., Guo, X., Luo, S., Yang, F., Feng, Y., Yang, G., and Liu, S. (2009). "Hydrogen-rich gas from catalytic steam gasification of municipal solid used (MSW): Influence of catalyst and temperature on yield and product composition," *Int. J. Hydrogen Energ.* 34(1), 195-203. DOI: 10.1016/j.ijhydene.2008.09.070

He, Y., Lin, H., Dong, Y., Li, B., Wang, L., Chu, S., Luo, M., and Liu, J. (2018). "Zeolite supported Fe/Ni bimetallic nanoparticles for simultaneous removal of nitrate and phosphate: Synergistic effect and mechanism," *Chem. Eng. J.* 347, 669-681. DOI: 10.1016/j.cej.2018.04.088

Hu, M., Laghari, M., Cui, B., Xiao, B., Zhang, B., and Guo, D. (2018). "Catalytic cracking of biomass tar over char supported nickel catalyst," *Energy* 145, 228-237. DOI: 10.1016/j.energy.2017.12.096

Hu, S., Jiang, L., Wang, Y., Su, S., Sun, L., Xu, B., He, L., and Xiang, J. (2015). "Effects of inherent alkali and alkaline earth metallic species on biomass pyrolysis at different temperatures," *Bioresource Technol.* 192, 23-30. DOI: 10.1016/j.biortech.2015.05.042

Kunkes, E. L., Simonetti, D. A., West, R. M., Serrano-Ruiz, J. C., Gärtner, C. A., and Dumesic, J. A. (2008). "Catalytic conversion of biomass to monofunctional hydrocarbons and targeted liquid-fuel classes," *Science* 322(5900), 417-421. DOI: 10.1126/science.1159210

Liu, H., Chen, T., Zhang, X., Li, J., Chang, D., and Song, L. (2010). "Effect of additives on catalytic cracking of biomass gasification tar over a nickel-based catalyst," *Chinese J. Catal.* 31(4), 409-414. DOI: 10.1016/s1872-2067(09)60061-9

Liu, W.-J., Zeng, F.-X., Jiang, H., and Zhang, X.-S. (2011). "Preparation of high adsorption capacity bio-chars from used biomass," *Bioresource Technol.* 102(17), 8247-8252. DOI: 10.1016/j.biortech.2011.06.014

Mazumder, J., and De Lasa, H. I. (2014). "Ni catalysts for steam gasification of biomass: Effect of La_2O_3 loading," *Catal. Today* 237, 100-110. DOI: 10.1016/j.cattod.2014.02.015

Paethanom, A., Nakahara, S., Kobayashi, M., Prawisudha, P. and Yoshikawa, K. (2012). "Performance of tar removal by absorption and adsorption for biomass gasification," *Fuel Process. Technol.* 104, 144-154. DOI: 10.1016/j.fuproc.2012.05.006

Paethanom, A., Bartocci, P., D' Alessandro, B., D' Amico, M., Testarmata, F., Moriconi, N., Slopiecka, K., Yoshikawa, K., and Fantozzi, F. (2013). "A low-cost pyrogas cleaning system for power generation: Scaling up from lab to pilot," *Appl. Energy* 111, 1080-1088. DOI: 10.1016/j.apenergy.2013.06.044

Shen, Y., Wang, J., Ge, X., and Chen, M. (2016). "By-products recycling for syngas cleanup in biomass pyrolysis – An overview," *Renew. Sust. Energ. Rev.* 59, 1246-1268. DOI: 10.1016/j.rser.2016.01.077

Shen, Y., Zhao, P., Shao, Q., Ma, D., Takahashi, F., and Yoshikawa, K. (2014). "*In-situ* catalytic conversion of tar using rice husk char-supported nickel-iron catalysts for biomass pyrolysis/gasification," *Appl. Catal. B Environ.* 152-153, 140-151. DOI: 10.1016/j.apcatb.2014.01.032

Sienkiewicz-Gromiuk, J., Rusinek, I., Kurach, Ł., and Rzączyńska, Z. (2016). "Thermal and spectroscopic (IR, XPS) properties of lanthanide(III) benzene-1,3,5-triacetate complexes," *J. Therm. Anal. Calorim.* 126(1), 327-342. DOI: 10.1007/s10973-016-5521-8

Sikarwar, V. S., Zhao, M., Clough, P., Yao, J., Zhong, X., Memon, M. Z., Shah, N., Anthony, E. J., and Fennell, P. S. (2016). "An overview of advances in biomass gasification," *Energ. Environ. Sci.* 9(10), 2939-2977. DOI: 10.1039/c6ee00935b

Valderrama Rios, M. L., González, A. M., Lora, E. E. S., and Almazán del Olmo, O. A. (2018). "Reduction of tar generated during biomass gasification: A review," *Biomass Bioenerg.* 108, 345-370. DOI: 10.1016/j.biombioe.2017.12.002

Xie, Y., Su, Y., Wang, P., Zhang, S., and Xiong, Y. (2018). "*In-situ* catalytic conversion of tar from biomass gasification over carbon nanofibers- supported Fe-Ni bimetallic catalysts," *Fuel Process. Technol.* 182, 77-87. DOI: 10.1016/j.fuproc.2018.10.019

Yamashita, T., and Hayes, P. (2008). "Analysis of XPS spectra of Fe^{2+} and Fe^{3+} ions in oxide materials," *Appl. Surf. Sci.* 254(8), 2441-2449. DOI: 10.1016/j.apsusc.2007.09.063

Yang, Y., Zhu, J., Zhu, G., Yang, L., and Zhu, Y. (2018). "The effect of high temperature on syngas production by immediate pyrolysis of wet sewage sludge with sawdust," *J. Therm. Anal. Calorim.* 132(3), 1783-1794. DOI: 10.1007/s10973-018-7143-9

Yao, D., Hu, Q., Wang, D., Yang, H., Wu, C., Wang, X., and Chen, H. (2016). "Hydrogen production from biomass gasification using biochar as a catalyst/support,"

Bioresource Technol. 216, 159-164. DOI: 10.1016/j.biortech.2016.05.011

Zeng, J., Xiao, R., Zhang, H., Chen, X., Zeng, D., and Ma, Z. (2017). "Syngas production *via* biomass self-moisture chemical looping gasification," *Biomass Bioenerg.* 104, 1-7. DOI: 10.1016/j.biombioe.2017.03.020

Zhu, J., Yang, Y., Yang, L., and Zhu, Y. (2018). "High quality syngas produced from the co-pyrolysis of wet sewage sludge with sawdust," *Int. J. Hydrogen Energ.* 43(11), 5463-5472. DOI: 10.1016/j.ijhydene.2018.01.171